Structural Studies of Amyloid Fibrils by Paramagnetic Solid-State Nuclear Magnetic Resonance Spectroscopy

Theint Theint,[†] Yongjie Xia,[†] Philippe S. Nadaud,[†] Dwaipayan Mukhopadhyay,[†]
Charles D. Schwieters,[‡] Krystyna Surewicz,[§] Witold K. Surewicz,[§] and Christopher P. Jaroniec*,[†]

[†]Department of Chemistry and Biochemistry, The Ohio State University, Columbus, Ohio 43210, United States
[‡]Center for Information Technology, National Institutes of Health, Bethesda, Maryland 20892, United States
[§]Department of Physiology and Biophysics, Case Western Reserve University, Cleveland, Ohio 44106, United States

Supporting Information Placeholder

ABSTRACT: Application of paramagnetic solid-state NMR to amyloids is demonstrated, using Y145Stop human prion protein modified with nitroxide spin-label or EDTA-Cu^{2+} tags as a model. By using sample preparation protocols based on seeding with pre-formed fibrils we show that paramagnetic protein analogs can be induced into adopting the wild-type amyloid structure. Measurements of residue-specific intramolecular and intermolecular paramagnetic relaxation enhancements enable determination of protein fold within the fibril core and protofilament assembly. These methods are expected to be widely applicable to other amyloids and protein assemblies.

Paramagnetism-based solid-state nuclear magnetic resonance (SSNMR) techniques yield site-specific electron-nucleus distances in the ~10-20 Å regime for biomacromolecules through measurements of nuclear pseudocontact shifts and spin relaxation enhancements.[1-5] To date, the utility of paramagnetic SSNMR in the context of three-dimensional protein structure determination, both *de novo* and in conjunction with conventional internuclear distance measurements, has been demonstrated for globular microcrystalline proteins including metalloproteins[6-8] and diamagnetic proteins tagged with paramagnetic side-chains.[9-13] Additionally, these methods have been successfully employed to probe structure and intermolecular interactions involving membrane proteins,[14-16] interactions between small molecules and lipids,[17] metal binding to membrane proteins and amyloids[18-20] and solvent-accessible surfaces in protein assemblies.[21-24]

One of the foremost challenges associated with structural studies of proteins by SSNMR methods based on paramagnetic tagging is that covalent linking of these moieties may significantly alter the native protein fold. To minimize the likelihood of such tag-induced structural perturbations, it is typical to target peripheral, solvent-exposed amino acids (aa), followed by comparison of NMR spectra for the wild-type (wt) protein and a diamagnetic analog of the paramagnetic mutant to confirm the absence of conformational changes.[25-27] However, for supramolecular assemblies such as amyloids—which are capable of adopting distinct structures in response to conservative mutations and/or other experimental factors,[28-30] and for which the locations of many residues within the structure and extent of their solvent accessibility may not be evident *a priori*—the placement of paramagnetic tags within the amyloid core in a manner that does not impact the native conformation presents a particularly acute challenge.

While for amyloids of unknown structure the selection of residues for paramagnetic tagging and subsequent SSNMR analysis inherently contains an element of guesswork, in many cases it may be possible to induce the tagged-proteins into adopting the native structure by using sample preparation protocols based on seeding with pre-formed fibrils of the wt protein[31] (even if these tagged-proteins are unable to assume the correct fold in the absence of seeding). Here, we demonstrate this concept for Y145Stop human prion protein (huPrP23-144) fibrils, followed by measurements of site-specific intramolecular and intermolecular paramagnetic relaxation enhancements (PREs) that yield valuable structural data. PrP23-144, which is associated with a heritable human prionopathy,[32] provides a useful *in vitro* model for studying the molecular basis of amyloid strains and cross-seeding barriers.[33-35] Our earlier studies of PrP23-144 amyloids[24,30,36-40] by SSNMR and other techniques, have shown that the structured core of huPrP23-144 fibrils consists of two protofilaments, with each protofilament containing a parallel-in-register β-sheet region spanning ~30 C-terminal residues (aa ~112-141) and the remainder of the protein effectively dynamically disordered.

To gain insight into the huPrP23-144 fold within protofilaments and the protofilament arrangement, we pursued measurements of long-range PRE-based structural restraints in fibrils modified with nitroxide spin-labels at

multiple locations.[25] Given the limited data about huPrP23-144 fibril structure available at the outset of these studies, we somewhat arbitrarily selected a set of five amyloid core residues to be substituted for cysteines by using site-directed mutagenesis and further modified with the thiol-specific spin-label reagent (1-oxyl-2,2,5,5-tetramethyl-Δ3-pyrroline-3-methyl)-methanethiosulfonate (side-chain R1)[41] as described in the Supporting Information (SI); for each spin-labeled protein, a diamagnetic reference sample was prepared by using an analogous methanethiosulfonate reagent containing a 1-acetyl group in place of 1-oxyl (side-chain R1').[42] The mutation sites (SI Figure S1) included three residues located near the edges of the amyloid core (aa 112, 113 and 141) and two additional residues in the core interior (aa 122 and 128).

Fibrils for SSNMR analysis of the protein fold within protofilaments were generated from physical mixtures of R1-tagged $^{13}C,^{15}N$-huPrP23-144 and natural abundance wt huPrP23-144 at ~30% dilution (see SI text), in order to minimize the influence of intermolecular electron-nucleus interactions.[25,43] We first investigated the possibility of growing fibrils, for several diamagnetic R1' mutants as test cases, using the usual protocol based on autocatalytic conformational conversion of huPrP23-144 under quiescent conditions at 25 °C.[40] While all mutants tested formed fibrils, none adopted the wt huPrP23-144 amyloid structure under these conditions. In Figure 1 we show a representative fingerprint 2D ^{15}N-$^{13}C\alpha$ SSNMR spectrum (see SI text) for 113R1' amyloid, which displays major differences relative to the corresponding spectrum for wt huPrP23-144 fibrils with respect to both the number of observable resonances and their ^{13}C and ^{15}N frequencies indicative of significant structural changes. Similar results were obtained for the other mutants including 122R1', 128R1' and 141R1' (SI Figure S1).

To investigate whether the observed spectral changes stem from changes in the aggregation mechanism due to covalent attachment of the R1/R1' tags within the amyloid core, we generated a control fibril sample under identical conditions using the 26R1' mutant, where the R1' side-chain is located near the dynamically disordered N-terminus[37] and far removed from the core. The spectrum of 26R1' fibrils (SI Figure S2) confirms that they adopt the wt huPrP23-144 structure. Remarkably, the fingerprint spectra of all the core R1' mutant fibrils generated using the autocatalytic method bear considerable similarity to one another and to huPrP23-144 A117V amyloid investigated in our earlier study.[30] While the high-resolution structure of the latter has not yet been determined, our initial data indicate that these fibrils differ significantly from huPrP23-144 amyloid and contain a β-sheet core that spans only ~15 residues (aa 122-137). Taken together with the present findings it appears that the amyloid core structure adopted by

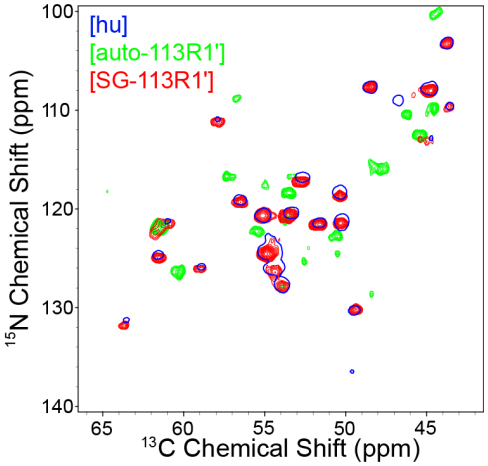

Figure 1. Two-dimensional ^{15}N-$^{13}C\alpha$ SSNMR spectra of 113R1' amyloid fibrils generated using the autocatalytic (green contours) and seeded growth (red contours) protocols, overlaid with the spectrum of native huPrP23-144 fibrils (single blue contour).

huPrP23-144 A117V represents a particularly stable fold for a number of PrP23-144 variants.

Given the ability of PrP23-144 and other amyloids to readily undergo cross-seeding reactions,[31,33-35] we next investigated the possibility of inducing huPrP23-144 R1/R1' mutants into adopting native-like structures in the fibrils by using a growth protocol where amyloid formation is accelerated by adding pre-formed wt huPrP23-144 fibril seeds (see SI text). We found that for three of the five mutants studied, including 113R1', 128R1' and 141R1', the use of this seeded growth (SG) protocol resulted in successful templating of the mutant protein by the native structure as evidenced by the similarity of wt and mutant chemical shifts in the 2D ^{15}N-$^{13}C\alpha$ spectra (Figure 1 and SI Figure S1). For 112R1' and 122R1' the seeding did not produce the desired effect, yielding amyloids with fingerprint spectra that were effectively identical to one another and to those for unseeded 122R1' fibrils (SI Figure S1). Interestingly, for 141R1' the SG method yielded samples containing a mixture of two fibril polymorphs, one with native structure and one corresponding to unseeded amyloid. In the context of this study, the concurrent presence of these polymorphs did not interfere with data analysis since they display largely distinct sets of chemical shifts in the 2D ^{15}N-$^{13}C\alpha$ spectra. In general, it is feasible that the population of undesirable structural polymorphs corresponding to the unseeded amyloid fold could be minimized by further optimization of the sample preparation conditions (e.g., increasing the seed concentration), but such fine tuning of the fibril growth was not pursued here. Note also that the ability of 113, 128 and 141R1/R1' mutants to adopt the native structure in seeded reactions carried out in presence of natural abundance wt huPrP23-144 in itself strongly suggests that the $^{13}C,^{15}N$-enriched paramagnetic proteins are randomly incorporated into the fibril lattice and diluted in a matrix

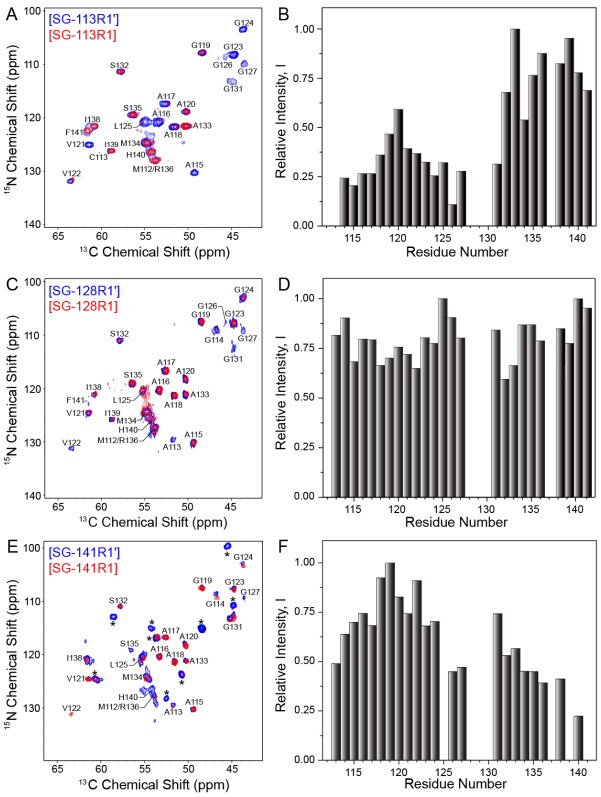

Figure 2. (A) Two-dimensional ^{15}N-^{13}Cα SSNMR spectra of 113R1 (red) and 113R1' (blue) fibrils. (B) ^{15}N-^{13}Cα cross-peak intensities reporting on intramolecular PREs as a function of residue number. To account for possible variation in the amount of ^{13}C,^{15}N-protein in paramagnetic and diamagnetic samples, relative intensities were calculated as: $I = (I_{para}/I_{dia})/(I_{para}/I_{dia})_{max}$, where I_{para} and I_{dia} are the peak intensities in R1 and R1' spectra and $(I_{para}/I_{dia})_{max}$ is the maximum (I_{para}/I_{dia}) value for the R1/R1' pair. For cross-peaks where no measurement was possible due to spectral overlap the relative intensity was set to zero. (C–F) Same as panels A,B but for 128R1/R1' and 141R1/R1'.

of diamagnetic protein on the molecular level. This was confirmed directly for one of the mutants (128R1) by recording electron paramagnetic resonance spectra for a series of fibril samples generated from physical mixtures of 128R1 and wt huPrP23-144 containing increasing amounts of the spin-labeled protein (SI Figure S3). Additionally, fibrillization kinetics for R1' mutants were investigated under SG conditions (SI Figure S4), but revealed no correlations with their ability to adopt wt huPrP23-144 amyloid structure.

In Figure 2 we show 2D ^{15}N-^{13}Cα spectra for the 113R1, 128R1 and 141R1 amyloids and their R1' counterparts, as well as plots of relative cross-peak intensities in paramagnetic and diamagnetic fibril samples. These data clearly show site-specific intramolecular transverse PRE effects reporting on the protein fold in the amyloid core as evidenced by the considerable attenuation of multiple cross-peak intensities, in analogy to earlier studies of spin-labeled globular proteins.[25] For 113R1 fibrils, residues ~113-117 and ~124-127 are most strongly attenuated, while somewhat less attenuation is observed on average for residues ~118-123 and significantly less for residues ~131-141. This indicates the presence of a turn-like motif, where the R1 side-chain at position 113 is located in close spatial proximity to aa ~124-127. For 128R1 fibrils, the absence of significant backbone PREs suggests that the R1 side-chain located in the relatively flexible loop region of the core points outward from the protofilament rather than being buried within it. Finally, for the 141R1 fibrils aa ~113-114 are significantly attenuated relative to the hydrophobic core residues ~118-122, suggesting that the N- and C-terminal edges of the amyloid core are located in the vicinity of one another and that the R1 side-chain in position 141 points toward the core interior.

In addition to probing the huPrP23-144 fold in the fibril core, we carried out analogous measurements of intermolecular PREs to characterize the protofilament assembly. Such measurements pose a considerable challenge for conventional SSNMR approaches, and, indeed, in none of our earlier studies of huPrP23-144 amyloid[30] have we been able to detect any unambiguous correlations reporting on through-space dipolar couplings between nuclei located in different protofilaments. Amyloid samples for the analysis of these intermolecular contacts were generated from physical mixtures of wt ^{13}C,^{15}N-huPrP23-144 and natural abundance R1-tagged huPrP23-144 at ~30% dilution (see SI text). In Figure 3, we show data for fibrils containing the R1 side-chain in position 128. While the observed attenuation of cross-peak intensities for residues ~125-127 could potentially be due to intermolecular contacts involving adjacent protein molecules within the parallel-in-register β-sheet protofilament,[38] the considerable attenuation of signals for aa ~113-115 must result from molecular level contacts between the two protofilaments given the large separation between these residues and the spin-label site within individual protofilaments. To further validate these interfilament contacts we carried out analogous experiments using fibrils containing EDTA-Cu^{2+} tags at residue 128 (SI Figures S5 and S6), and found that residues ~113-115 which display large transverse PREs in the spin-labeled fibrils also show the largest longitudinal ^{15}N PREs with the EDTA-Cu^{2+} tags.

To assess the utility of PRE-based restraints for determining the fold of huPrP23-144 and protofilament arrangement within the fibril core we carried out a set of structure calculations based on these data in Xplor-NIH[44] (see SI text). Figure 3C shows the resulting ensemble of ten low-energy backbone structures for huPrP23-144 residues 109-144 corresponding to one layer of the two protofilament assembly, with SI Figure S7 showing the same ensemble of structures aligned within each protofilament. While this structural ensemble is relatively low resolution, which is to be expected given the sparseness and semi-quantitative nature of the nitroxide spin-label-based PRE restraints in this study, it is clearly able to delineate the overall huPrP23-144 fibril

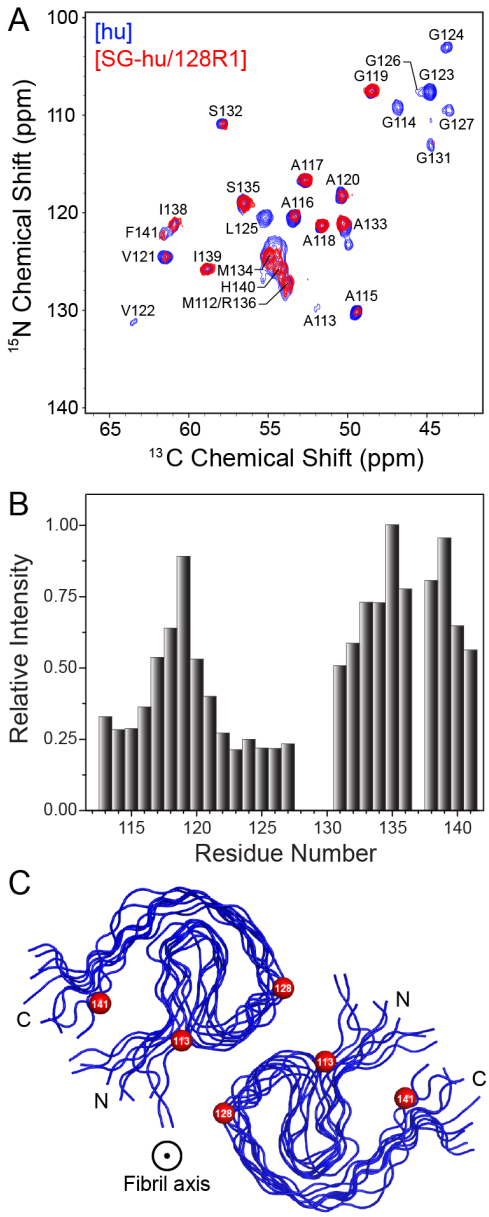

Figure 3. (A) Two-dimensional ^{15}N-^{13}Cα SSNMR spectra of ^{13}C,^{15}N-huPrP23-144 fibrils containing ~30% natural abundance 128R1 (red) and reference ^{13}C,^{15}N-huPrP23-144 fibrils (blue). (B) ^{15}N-^{13}Cα cross-peak intensities reporting on intermolecular PREs (see Figure 2 caption). (C) Ensemble of ten low-energy backbone structures for huPrP23-144 residues 109-144 corresponding to one layer of the two protofilament assembly (see SI text and Figure S7). Paramagnetic-tagged residues are indicated by red spheres.

conformation. Most importantly, the PRE-derived structural model in Figure 3C is consistent with and expands on our earlier preliminary studies of huPrP23-144 amyloid by SSNMR and electron microscopy[30] and provides a firm foundation for high-resolution structure determination.

In summary, we have demonstrated measurements of intramolecular and intermolecular PREs in huPrP23-144 fibrils containing spin-label or EDTA-Cu^{2+} tags. These measurements provide valuable information about amyloid structure, including data inaccessible by conventional SSNMR, and, remarkably, enable the determination of the protein fold in the huPrP23-144 amyloid core and protofilament assembly. This methodology is expected to be broadly applicable to other amyloid-forming proteins and can be further extended to other types of paramagnetic tags[11,45] and by incorporating rapid sample spinning and proton detection[13,46] for improved sensitivity.

ASSOCIATED CONTENT

Supporting Information

The Supporting Information is available free of charge on the ACS Publications website at DOI: XXXXX

Materials and Methods section, figures with NMR and EPR spectra, thioflavin T fluorescence assays, structure calculations (PDF)

AUTHOR INFORMATION

Corresponding Author

*jaroniec.1@osu.edu

ORCID

Christopher P. Jaroniec: 0000-0003-0364-2888

Notes

The authors declare no competing financial interests.

ACKNOWLEDGMENTS

This work was supported by the National Science Foundation (grants MCB-1243461 and MCB-1715174 to C.P.J.), the National Institutes of Health (grants R01GM094357, R01GM118664, R01GM123743 and S10OD012303 to C.P.J. and P01AI106705 and R01NS083687 to W.K.S.) and the Camille & Henry Dreyfus Foundation (Camille Dreyfus Teacher-Scholar Award to C.P.J.). C.D.S. was supported by the NIH Intramural Research Program of the Center for Information Technology.

REFERENCES

(1) Pintacuda, G.; Kervern, G. Paramagnetic solid-state magic-angle spinning NMR spectroscopy. *Top. Curr. Chem.* **2012,** *335*, 157-200.

(2) Jaroniec, C. P. Solid-state nuclear magnetic resonance structural studies of proteins using paramagnetic probes. *Solid State Nucl. Magn. Reson.* **2012,** *43-44*, 1-13.

(3) Bhaumik, A.; Luchinat, C.; Parigi, G.; Ravera, E.; Rinaldelli, M. NMR crystallography on paramagnetic systems: Solved and open issues. *CrystEngComm* **2013,** *15*, 8639-8656.

(4) Knight, M. J.; Felli, I. C.; Pierattelli, R.; Emsley, L.; Pintacuda, G. Magic angle spinning NMR of paramagnetic proteins. *Acc. Chem. Res.* **2013,** *46*, 2108-2116.

(5) Jaroniec, C. P. Structural studies of proteins by paramagnetic solid-state NMR spectroscopy. *J. Magn. Reson.* **2015,** *253*, 50-59.

(6) Bertini, I.; Bhaumik, A.; De Paëpe, G.; Griffin, R. G.; Lelli, M.; Lewandowski, J. R.; Luchinat, C. High-resolution solid-state NMR structure of a 17.6 kDa protein. *J. Am. Chem. Soc.* **2010,** *132*, 1032-1040.

(7) Knight, M. J.; Pell, A. J.; Bertini, I.; Felli, I. C.; Gonnelli, L.; Pierattelli, R.; Herrmann, T.; Emsley, L.; Pintacuda, G. Structure and backbone dynamics of a microcrystalline metalloprotein by solid-state NMR. *Proc. Natl. Acad. Sci. USA* **2012,** *109*, 11095-11100.

(8) Luchinat, C.; Parigi, G.; Ravera, E.; Rinaldelli, M. Solid-state NMR crystallography through paramagnetic restraints. *J. Am. Chem. Soc.* **2012,** *134*, 5006-5009.
(9) Sengupta, I.; Nadaud, P. S.; Helmus, J. J.; Schwieters, C. D.; Jaroniec, C. P. Protein fold determined by paramagnetic magic-angle spinning solid-state NMR spectroscopy. *Nat. Chem.* **2012,** *4*, 410-417.
(10) Sengupta, I.; Nadaud, P. S.; Jaroniec, C. P. Protein structure determination with paramagnetic solid-state NMR spectroscopy. *Acc. Chem. Res.* **2013,** *46*, 2117-2126.
(11) Li, J.; Pilla, K. B.; Li, Q.; Zhang, Z.; Su, X.; Huber, T.; Yang, J. Magic angle spinning NMR structure determination of proteins from pseudocontact shifts. *J. Am. Chem. Soc.* **2013,** *135*, 8294-8303.
(12) Tamaki, H.; Egawa, A.; Kido, K.; Kameda, T.; Kamiya, M.; Kikukawa, T.; Aizawa, T.; Fujiwara, T.; Demura, M. Structure determination of uniformly ^{13}C,^{15}N labeled protein using qualitative distance restraints from MAS solid-state ^{13}C-NMR observed paramagnetic relaxation enhancement. *J. Biomol. NMR* **2016,** *64*, 87-101.
(13) Rovo, P.; Grohe, K.; Giller, K.; Becker, S.; Linser, R. Proton transverse relaxation as a sensitive probe for structure determination in solid proteins. *Chemphyschem* **2015,** *16*, 3791-6.
(14) Wang, S.; Munro, R. A.; Kim, S. Y.; Jung, K.-H.; Brown, L. S.; Ladizhansky, V. Paramagnetic relaxation enhancement reveals oligomerization interface of a membrane protein. *J. Am. Chem. Soc.* **2012,** *134*, 16995-16998.
(15) Gustavsson, M.; Verardi, R.; Mullen, D. G.; Mote, K. R.; Traaseth, N. J.; Gopinath, T.; Veglia, G. Allosteric regulation of SERCA by phosphorylation-mediated conformational shift of phospholamban. *Proc. Natl. Acad. Sci. USA* **2013,** *110*, 17338-43.
(16) van der Cruijsen, E. A.; Koers, E. J.; Sauvee, C.; Hulse, R. E.; Weingarth, M.; Ouari, O.; Perozo, E.; Tordo, P.; Baldus, M. Biomolecular DNP-Supported NMR Spectroscopy using Site-Directed Spin Labeling. *Chem. Eur. J.* **2015,** *21*, 12971-12977.
(17) Anderson, T. M.; Clay, M. C.; Cioffi, A. G.; Diaz, K. A.; Hisao, G. S.; Tuttle, M. D.; Nieuwkoop, A. J.; Comellas, G.; Maryum, N.; Wang, S.; Uno, B. E.; Wildeman, E. L.; Gonen, T.; Rienstra, C. M.; Burke, M. D. Amphotericin forms an extramembranous and fungicidal sterol sponge. *Nat. Chem. Biol.* **2014,** *10*, 400-406.
(18) Su, Y.; Hu, F.; Hong, M. Paramagnetic Cu(II) for probing membrane protein structure and function: inhibition mechanism of the influenza M2 proton channel. *J. Am. Chem. Soc.* **2012,** *134*, 8693-8702.
(19) Parthasarathy, S.; Long, F.; Miller, Y.; Xiao, Y.; McElheny, D.; Thurber, K.; Ma, B.; Nussinov, R.; Ishii, Y. Molecular-level examination of Cu^{2+} binding structure for amyloid fibrils of 40-residue Alzheimer's β by solid-state NMR spectroscopy. *J. Am. Chem. Soc.* **2011,** *133*, 3390-3400.
(20) Parthasarathy, S.; Yoo, B.; McElheny, D.; Tay, W.; Ishii, Y. Capturing a reactive state of amyloid aggregates: NMR-based characterization of copper-bound Alzheimer disease amyloid β-fibrils in a redox cycle. *J. Biol. Chem.* **2014,** *289*, 9998-10010.
(21) Wickramasinghe, N. P.; Parthasarathy, S.; Jones, C. R.; Bhardwaj, C.; Long, F.; Kotecha, M.; Mehboob, S.; Fung, L. W. M.; Past, J.; Samoson, A.; Ishii, Y. Nanomole-scale protein solid-state NMR by breaking intrinsic ^{1}H T_1 boundaries. *Nat. Methods* **2009,** *6* 215-218.
(22) Linser, R.; Fink, U.; Reif, B. Probing surface accessibility of proteins using paramagnetic relaxation in solid-state NMR spectroscopy. *J. Am. Chem. Soc.* **2009,** *131*, 13703-13708.
(23) Oster, C.; Kosol, S.; Hartlmuller, C.; Lamley, J. M.; Iuga, D.; Oss, A.; Org, M. L.; Vanatalu, K.; Samoson, A.; Madl, T.; Lewandowski, J. R. Characterization of protein-protein interfaces in large complexes by solid-state NMR solvent paramagnetic relaxation enhancements. *J. Am. Chem. Soc.* **2017,** *139*, 12165-12174.
(24) Aucoin, D.; Xia, Y.; Theint, T.; Nadaud, P. S.; Surewicz, K.; Surewicz, W. K.; Jaroniec, C. P. Protein-solvent interfaces in Y145Stop human prion protein amyloid fibrils probed by paramagnetic solid-state NMR spectroscopy. *J. Struct. Biol.* **2018**, published online, doi: 10.1016/j.jsb.2018.04.002.
(25) Nadaud, P. S.; Helmus, J. J.; Höfer, N.; Jaroniec, C. P. Long-range structural restraints in spin-labeled proteins probed by solid-state nuclear magnetic resonance spectroscopy. *J. Am. Chem. Soc.* **2007,** *129*, 7502-7503.
(26) Nadaud, P. S.; Helmus, J. J.; Kall, S. L.; Jaroniec, C. P. Paramagnetic ions enable tuning of nuclear relaxation rates and provide long-range structural restraints in solid-state NMR of proteins. *J. Am. Chem. Soc.* **2009,** *131*, 8108-8120.
(27) Nadaud, P. S.; Helmus, J. J.; Sengupta, I.; Jaroniec, C. P. Rapid acquisition of multidimensional solid-state NMR spectra of proteins facilitated by covalently bound paramagnetic tags. *J. Am. Chem. Soc.* **2010,** *132*, 9561-9563.
(28) Tycko, R. Molecular Structure of Aggregated Amyloid-β: Insights from Solid-State Nuclear Magnetic Resonance. *Cold Spring Harb. Perspect. Med.* **2016,** *6*, a024083.
(29) Riek, R.; Eisenberg, D. S. The activities of amyloids from a structural perspective. *Nature* **2016,** *539*, 227-235.
(30) Theint, T.; Nadaud, P. S.; Aucoin, D.; Helmus, J. J.; Pondaven, S. P.; Surewicz, K.; Surewicz, W. K.; Jaroniec, C. P. Species-dependent structural polymorphism of Y145Stop prion protein amyloid revealed by solid-state NMR spectroscopy. *Nat. Commun.* **2017,** *8*, 753.
(31) Petkova, A. T.; Leapman, R. D.; Guo, Z. H.; Yau, W. M.; Mattson, M. P.; Tycko, R. Self-propagating, molecular-level polymorphism in Alzheimer's β-amyloid fibrils. *Science* **2005,** *307*, 262-265.
(32) Ghetti, B.; Piccardo, P.; Spillantini, M. G.; Ichimiya, Y.; Porro, M.; Perini, F.; Kitamoto, T.; Tateishi, J.; Seiler, C.; Frangione, B.; Bugiani, O.; Giaccone, G.; Prelli, F.; Goedert, M.; Dlouhy, S. R.; Tagliavini, F. Vascular variant of prion protein cerebral amyloidosis with τ-positive neurofibrillary tangles: The phenotype of the stop codon 145 mutation in PRNP. *Proc. Natl. Acad. Sci. USA* **1996,** *93*, 744-748.
(33) Kundu, B.; Maiti, N. R.; Jones, E. M.; Surewicz, K. A.; Vanik, D. L.; Surewicz, W. K. Nucleation-dependent conformational conversion of the Y145Stop variant of human prion protein: Structural clues for prion propagation. *Proc. Natl. Acad. Sci. USA* **2003,** *100*, 12069-12074.
(34) Vanik, D. L.; Surewicz, K. A.; Surewicz, W. K. Molecular basis of barriers for interspecies transmissibility of mammalian prions. *Mol. Cell* **2004,** *14*, 139-145.
(35) Jones, E. M.; Surewicz, W. K. Fibril conformation as the basis of species- and strain-dependent seeding specificity of mammalian prion amyloids. *Cell* **2005,** *121*, 63-72.
(36) Helmus, J. J.; Surewicz, K.; Nadaud, P. S.; Surewicz, W. K.; Jaroniec, C. P. Molecular conformation and dynamics of the Y145Stop variant of human prion protein in amyloid fibrils. *Proc. Natl. Acad. Sci. USA* **2008,** *105*, 6284-6289.
(37) Helmus, J. J.; Surewicz, K.; Surewicz, W. K.; Jaroniec, C. P. Conformational flexibility of Y145Stop human prion protein amyloid fibrils probed by solid-state nuclear magnetic resonance spectroscopy. *J. Am. Chem. Soc.* **2010,** *132*, 2393-2403.
(38) Helmus, J. J.; Surewicz, K.; Apostol, M. I.; Surewicz, W. K.; Jaroniec, C. P. Intermolecular alignment in Y145Stop human prion protein amyloid fibrils probed by solid-state NMR spectroscopy. *J. Am. Chem. Soc.* **2011,** *133*, 13934-13937.
(39) Jones, E. M.; Wu, B.; Surewicz, K.; Nadaud, P. S.; Helmus, J. J.; Chen, S.; Jaroniec, C. P.; Surewicz, W. K. Structural polymorphism in amyloids: New insights from studies with Y145Stop prion protein fibrils. *J. Biol. Chem.* **2011,** *286*, 42777-42784.
(40) Theint, T.; Nadaud, P. S.; Surewicz, K.; Surewicz, W. K.; Jaroniec, C. P. ^{13}C and ^{15}N chemical shift assignments of mammalian Y145Stop prion protein amyloid fibrils. *Biomol. NMR Assign.* **2017,** *11*, 75-80.
(41) Berliner, L. J.; Grunwald, J.; Hankovszky, H. O.; Hideg, K. A novel reversible thiol-specific spin label: papain active site labeling and inhibition. *Anal. Biochem.* **1982,** *119*, 450-455.
(42) Gross, A.; Columbus, L.; Hideg, K.; Altenbach, C.; Hubbell, W. L. Structure of the KcsA potassium channel from Streptomyces lividans: A site-directed spin labeling study of the second transmembrane segment. *Biochemistry* **1999,** *38*, 10324-10335.
(43) Nadaud, P. S.; Sengupta, I.; Helmus, J. J.; Jaroniec, C. P. Evaluation of the influence of intermolecular electron-nucleus couplings and intrinsic metal binding sites on the measurement of ^{15}N longitudinal paramagnetic relaxation enhancements in proteins by solid-state NMR. *J. Biomol. NMR* **2011,** *51*, 293-302.
(44) Schwieters, C. D.; Bermejo, G. A.; Clore, G. M. Xplor-NIH for molecular structure determination from NMR and other data sources. *Protein Sci.* **2018,** *27*, 26-40.
(45) Sengupta, I.; Gao, M.; Arachchige, R. J.; Nadaud, P. S.; Cunningham, T. F.; Saxena, S.; Schwieters, C. D.; Jaroniec, C. P. Protein structural studies by paramagnetic solid-state NMR

spectroscopy aided by a compact cyclen-type Cu(II) binding tag. *J. Biomol. NMR* **2015,** *61*, 1-6.
(46) Mukhopadhyay, D.; Nadaud, P. S.; Shannon, M. D.; Jaroniec, C. P. Rapid Quantitative Measurements of Paramagnetic Relaxation Enhancements in Cu(II)-Tagged Proteins by Proton-Detected Solid-State NMR Spectroscopy. *J. Phys. Chem. Lett.* **2017,** *8*, 5871-5877.

TOC Graphic